Materials Science and Engineering A 508 (2009) 209–213

Contents lists available at ScienceDirect

Materials Science and Engineering A

journal homepage: www.elsevier.com/locate/msea

Microstructures and tensile deformation behavior of Cu–16 wt.%Ag binary alloy

Y.Z. Tian, Z.F. Zhang*

Shenyang National Laboratory for Materials Science, Institute of Metal Research, Chinese Academy of Sciences, 72 Wenhua Road, Shenyang 110016, PR China

ARTICLE INFO

Article history:
Received 6 October 2008
Received in revised form 17 December 2008
Accepted 22 December 2008

Keywords:
Cu–Ag alloy
Microstructure
Tensile deformation
Precipitates
Eutectic
Slip bands

ABSTRACT

The microstructures and tensile deformation behavior of Cu–16 wt.%Ag binary alloy with coarse grains were investigated by electron backscattered diffraction (EBSD) and scanning electron microscope (SEM). No precipitate was found in both eutectic Cu and Ag phases, whereas abundant precipitates were observed in proeutectic Cu matrix. Slip bands appear in the dendrites, though they are abundant in precipitates, and this can be attributed to the cube-on-cube orientation relationship and the coplanar slip systems between them. Slip bands can penetrate continuously through the eutectic region and the dendrites. The EBSD results revealed that they always had the same orientation. The tensile stress–strain curves displayed certain work-hardening behavior and high elongation. The highly continuous slip deformation mode and the good strain compatibility between matrix and the eutectic region will be beneficial to the high elongation of the Cu–Ag alloy.

1. Introduction

Cu and Ag are all face-centered cubic (fcc) metals, with lattice parameters of 0.3615 and 0.4086 nm, respectively. In particular, they belong to the same main group in the periodic table, and both show good conductivity and super-high plastic deformation ability [1]. Therefore, this gives rise to an interesting question: whether one can fabricate some Cu–Ag binary alloys with high strength, good conductivity and elongation? Recently, some investigators have devoted to develop the Cu–Ag alloys for the application in high-field magnets [2–5]. During cold drawing and appropriate intermediate heat treatment, some Cu–Ag composites with high strength and high conductivity have been obtained [6–10]. However, in those Cu–Ag alloys, the fundamental plastic deformation mechanisms were not well investigated though they provided some data about the mechanical properties. To obtain superior property in the future, it is rather important to investigate the microstructures and the mechanical response of Cu–Ag binary alloys first.

The phase diagram of Cu–Ag binary alloy is shown in Fig. 1 [11]. The volume fraction of the eutectic region increases with the Ag content for the Cu–Ag binary alloy, and the morphology changes correspondingly [12]. There were some experimental observations on the orientation relationship between the precipitates and the dendrites in Cu–Ag alloys previously [13–15]. Besides, the cube-on-cube orientation relationship was also found to exist between Cu matrix and Ag filament in the heavily drawn Cu–Ag microcomposites [16,17]. Whereas the microstructure and the strengthening effects of interphase interfaces were discussed previously [18–22].

In the current study, a Cu–16 wt.%Ag binary alloy was prepared under the furnace cooling condition to obtain coarse-grained microstructures, because the active slip bands in matrix and eutectic can be clearly observed, and this will enable us to investigate the basic deformation mechanism conveniently. The present work was conducted to gain understanding of the nucleation mechanism and investigate the mechanical response of the eutectic region and the dendrites. Furthermore, this will play an important role in understanding the toughening mechanism and the optimized mechanical properties of Cu–Ag binary alloy in the future.

2. Experimental procedures

The starting materials are OFHC Cu of 99.999% purity and electrolytic Ag of 99.99% purity, respectively. Then, a Cu–Ag alloy plate with a dimension of 40 mm × 15 mm × 150 mm was molten at a temperature of 1200 °C by the Bridgman method with a graphite crucible in a horizontal furnace [23]. When the heating process was over, the furnace was switched off, and the Cu–Ag alloy began to solidify with temperature decreasing. Since the weight loss was negligible during casting, the nominal compositions of Cu–16 wt.%Ag (see the broken line in Fig. 1) could be regarded as the true composition in the current study. Further element analysis by energy dispersive X-ray spectroscopy (EDX) indicated that the average composition was well consistent with the nominal composition (see Table 1). The alloy was used directly without heat treatment since the cooling rate was slow enough. The samples

* Corresponding author. Tel.: +86 24 23971043.
E-mail address: zhfzhang@imr.ac.cn (Z.F. Zhang).

0921-5093/$ – see front matter © 2009 Elsevier B.V. All rights reserved.
doi:10.1016/j.msea.2008.12.050

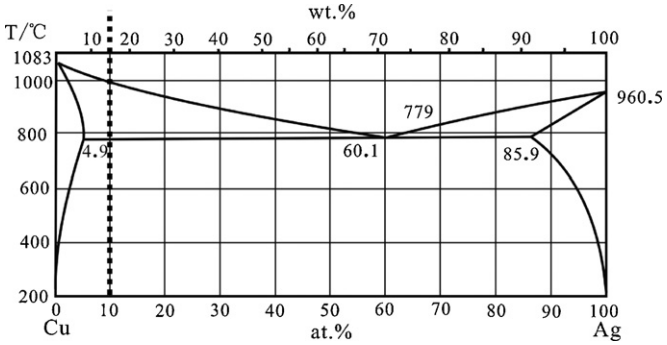

Fig. 1. Phase diagram of Cu–Ag binary alloy [11].

Table 1
Chemical composition of the Cu–Ag alloy.

	Cu (at.%)	Cu (wt.%)	Ag (at.%)	Ag (wt.%)
Nominal composition	90	84.1	10.00	15.9
True composition	90.2 ± 0.5	84.4 ± 0.5	9.8 ± 0.5	15.6 ± 0.5

were ground and polished first, then etched in a solution of 2 g $FeCl_3$, 5 ml HCl, and 100 ml C_2H_5OH, and observed by optical microscope and scanning electron microscope (SEM).

Since Cu–Ag hypoeutectic alloys contain Ag and Cu phases, the difference in electropolishing rate results in difficult sample preparation. Up to now, a proper electropolishing solution has not been found yet. In order to obtain a flatter surface and thus enable area measurement of orientations for EBSD mapping, an ion milling method was developed [24]. A slice of the alloy was ground and polished to a thickness less than 200 μm first, and then some EBSD samples of 3 mm in diameter were punched for ion milling. The ion milling conditions were as below: 1.5 h at a voltage of 4 kV and gun tilt angle of 15°, followed by 0.5 h at a gun tilt angle of 12°, and with cooling by liquid nitrogen during milling. Finally, the samples were observed by LEO SUPRA 35 SEM equipped with an EBSD system.

The tensile specimens with a gauge dimension of 16 mm × 5 mm × 4 mm and a total length of 60 mm were machined by spark-cutting technique. Before tensile deformation, all the specimens were ground and polished carefully for surface observation. Tensile tests were performed using an Instron 8871 testing machine at a nominal strain rate of about 5×10^{-4} s^{-1}. After tension, the specimens were observed by using SEM to reveal the surface deformation morphologies and fracture behavior.

3. Results and discussion

3.1. Microstructures

For hypoeutectic Cu–Ag binary alloy (see Fig. 1), when the Ag content is low, the eutectic colonies disperse as isolated islands in the interdendritic spaces. Whereas increasing the Ag content, the percentage of eutectic region increases too, as shown in Fig. 2a. The eutectic region shows a continuous net-like distribution between the dendritic arms [12]. Though the grain sizes are not uniformly distributed (the biggest one is ~5 mm), it was very helpful to investigate the mechanical response of the eutectic and the dendrite (see the next section). Grain boundaries are missing, because the high volume fraction of the eutectic reduces the probability that two dendrites directly adjoin each other during solidification [25], but the dendrites have slight difference in contrast. Here, the boundary of two regions with different orientations is still defined as grain boundary in order to facilitate the description and discussion later. Generally, the dendritic arm spacing is related to the cooling rate, and changes insignificantly with Ag content [6]. In the present work, the dendritic arm spacing is estimated to be 60–180 μm, which is much bigger than that reported before [6,7,10,12,13,25].

Fig. 2b shows the typical microstructure of etched Cu–16 wt.%Ag alloy taken by SEM. No precipitate is found in both eutectic Cu and Ag phases, whereas abundant Ag precipitates are observed in the proeutectic Cu matrix. The disappearance of Ag precipitates in the eutectic region can be attributed to the short distance between the Cu and Ag phases, so the Cu and Ag atoms can diffuse into the corresponding phase, in that case, no precipitate appears with

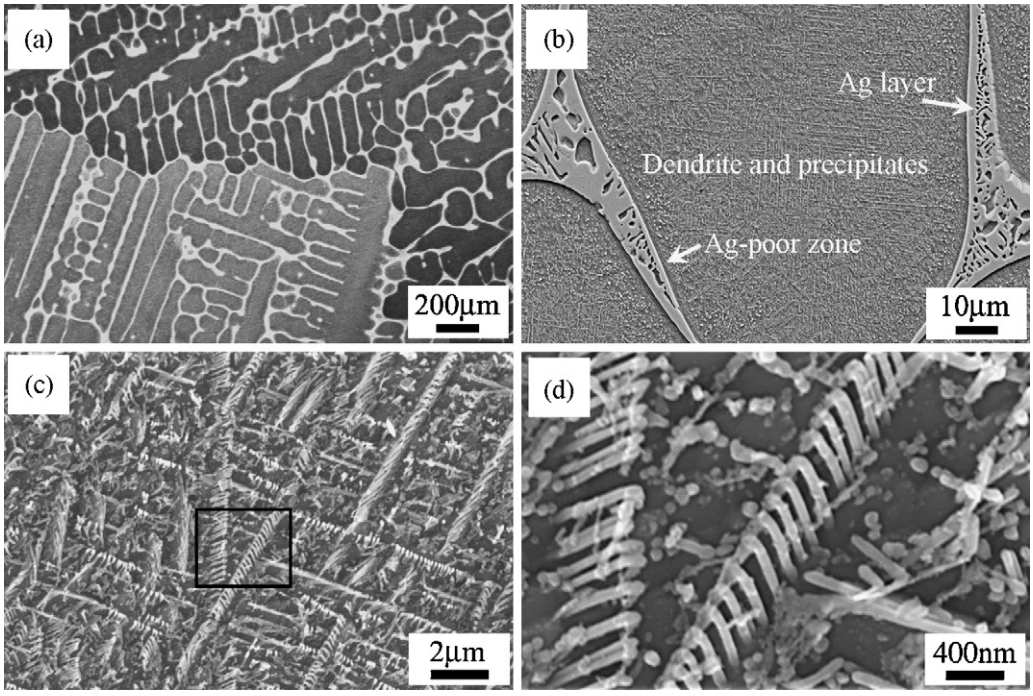

Fig. 2. Microstructures of the Cu–16 wt.%Ag alloy: (a) taken by optical microscopy and (b–d) taken by SEM at different magnitudes.

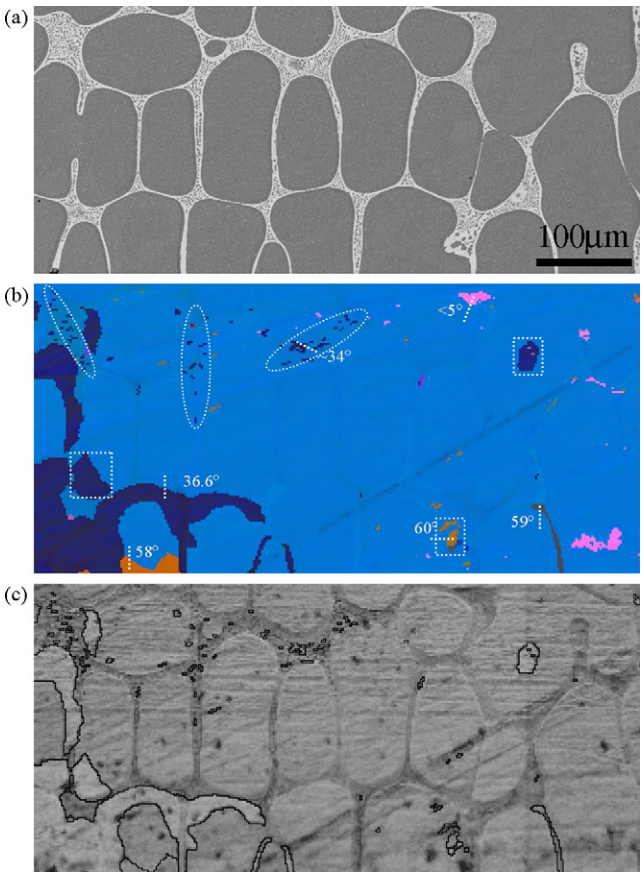

Fig. 3. (a) SEM backscatter diffraction image, (b) EBSD orientation map of the same area and (c) Kikuchi band contrast and high angle boundary map of the same area of the Cu–16 wt.%Ag alloy.

temperature decreasing. In addition, it is observed that a thick Ag layer encloses on the external surface of the eutectic region. In the vicinity of the Ag layer, there is a Ag-poor zone [13]. A possible explanation is as follows: because of the chemical potential difference between the dendrite and the eutectic region, the partitioning of Ag into eutectic region and Cu into dendrite close to the interface is a result of inter-diffusion after the eutectic region has solidified. The result would be a depletion of Ag in the boundary layer of the dendrite plus an enrichment of Ag in the boundary layer of the eutectic region. Fig. 2c shows the rod-like precipitates in the proeutectic Cu matrix. At higher magnification, as shown in Fig. 2d, it is clearly seen that a line of rod-like precipitates distributed regularly, with average diameter of about 50–90 nm. These rod-like precipitates are arranged closely, and their diameters are nearly the same as the spacing, as a result, they cannot be distinguished clearly at lower magnification.

Fig. 3a–c shows the SEM backscattered diffraction image, EBSD orientation map, Kikuchi band contrast and high angle boundary map, respectively. The misorientation angles were labeled on the EBSD orientation map, as shown in Fig. 3b, whereas Fig. 3c shows the high angle boundary with angles higher than 15°. Mostly, it is found that the eutectic region and the dendrites have the same orientation. Supposing that there are three proposed eutectic nucleation and growth modes [26], i.e. (1) nucleation at or adjacent to the mould wall and front growth opposite the thermal gradient, (2) nucleation of eutectic region on primary dendrites, and (3) heterogeneous nucleation of eutectic region on nucleation particles in the interdendritic liquid. So in the current study, the second nucleation and growth mode may be the predominant one. Interestingly, in some areas of the eutectic colony, the Cu and Ag phases show

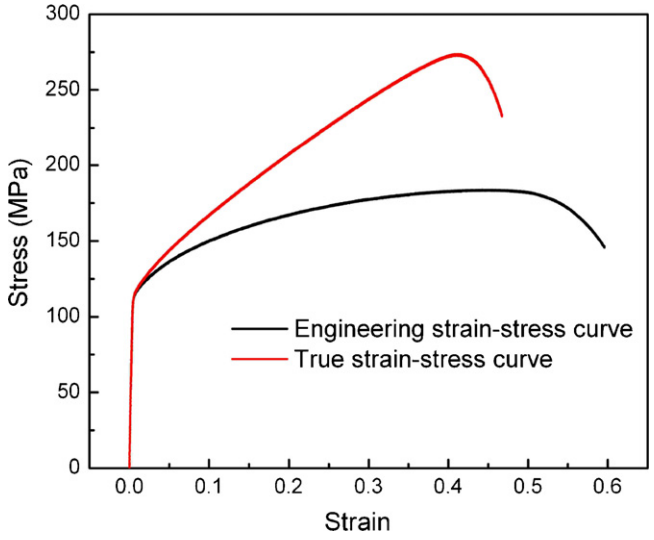

Fig. 4. Engineering and true tensile stress–strain curves of the Cu–16 wt.%Ag alloy at a strain rate of $5 \times 10^{-4}\ s^{-1}$.

other orientations (see inset ellipse in Fig. 3b). In Al–Si hypoeutectic alloy, it was hypothesized that the appearance of eutectic aluminum with other orientations might result from encountering solidifying from eutectic growing in the third dimension or possibly by re-nucleation on the leading silicon phase during eutectic growth [27]. In the current Cu–16 wt.%Ag alloy, the appearance of the eutectic colony with other orientation does not seem to result from the homogeneous nucleation, as the homogeneous nucleation energy barrier is high enough [28,29]. Besides, such areas distributed widely and did not grow big enough though the cooling rate is very slow. So the Cu and Ag phases inside the eutectic colony may have the same orientation, or show no orientation relationship [13]. What is more, some regions with high misorientation angles inside the dendrites were found (see inset rectangle in Fig. 3b). This can be attributed to the missing of the eutectic colony in the interdendritic region during solidification.

3.2. Tensile properties and plastic deformation behaviors

Based on the understanding of the microstructures of Cu–16 wt.%Ag binary alloy, tensile test was performed to investigate the mechanical property and plastic deformation behaviors. Fig. 4 shows the engineering and true tensile strain–stress curves, it appears that the Cu–Ag alloy only displays a relatively low tensile strength, but has a good elongation as high as ~50%, which can be attributed to the coarse-grained microstructure obtained at slow cooling rate. In the hypoeutectic Cu–Ag alloy, the eutectic colonies disperse between the dendritic arms and the grain boundaries after the solidification of dendrites. Different solidifying sequences and growth conditions result in the eutectic colonies with different characters. So the mechanical response and the tensile deformation morphologies were investigated after loading.

The Cu–16 wt.%Ag alloy undergoes the uniform plastic deformation and local necking before final fracture, as shown in Fig. 5a. Since the deformation degree differs in different regions, generally, we can divide the deformation surface of the specimen into two regions, i.e. uniform deformation region (U) and necking region (N), respectively.

Fig. 5b–d shows the surface deformation morphologies in region N. The eutectic colonies are elongated along the loading direction due to the necking process, as shown in Fig. 5b. Meanwhile, multiple slip bands are activated within the matrix (see Fig. 5c). In most of the grains, two sets of slip systems are stimulated to form the

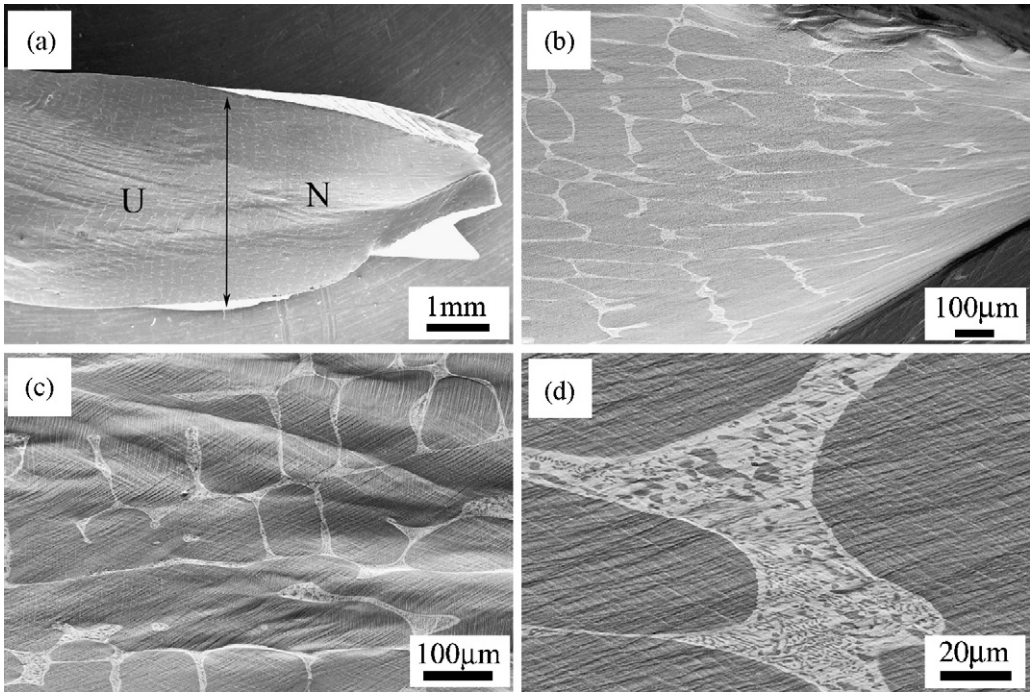

Fig. 5. (a) SEM images showing the slip morphologies and (b–d) surface deformation morphologies in region N of the Cu–16 wt.%Ag alloy.

intersecting slip bands. Since region N of the specimen is distorted due to necking, even in the same grain, the deformation morphologies are still inhomogeneous. Though the dendrites are abundant in precipitates, slip bands still appear. This can be attributed to the cube-on-cube orientation relationship [13–15] and the coplanar slip systems between the precipitates and the dendrites; besides, there are some slip bands within the eutectic region, as shown in Fig. 5d.

In the uniform deformation region U, it is very helpful to investigate the plastic deformation mechanism because the surface deformation is much more stable than that in region N. Fig. 6a shows the slip morphologies on both sides of a grain boundary. It is found that only primary slip system is activated in grain A, while in grain B, some secondary slip bands appear near the grain boundary. The detailed deformation morphology is revealed, as shown in Fig. 6b. Above the white broken line, the slip direction of the eutectic region is identical to that in grain A, whereas the slip bands in grain B can pass through the eutectic region below the broken line, and terminate at the interphase interface, indicating that the upper and lower eutectic regions may have the same orientation

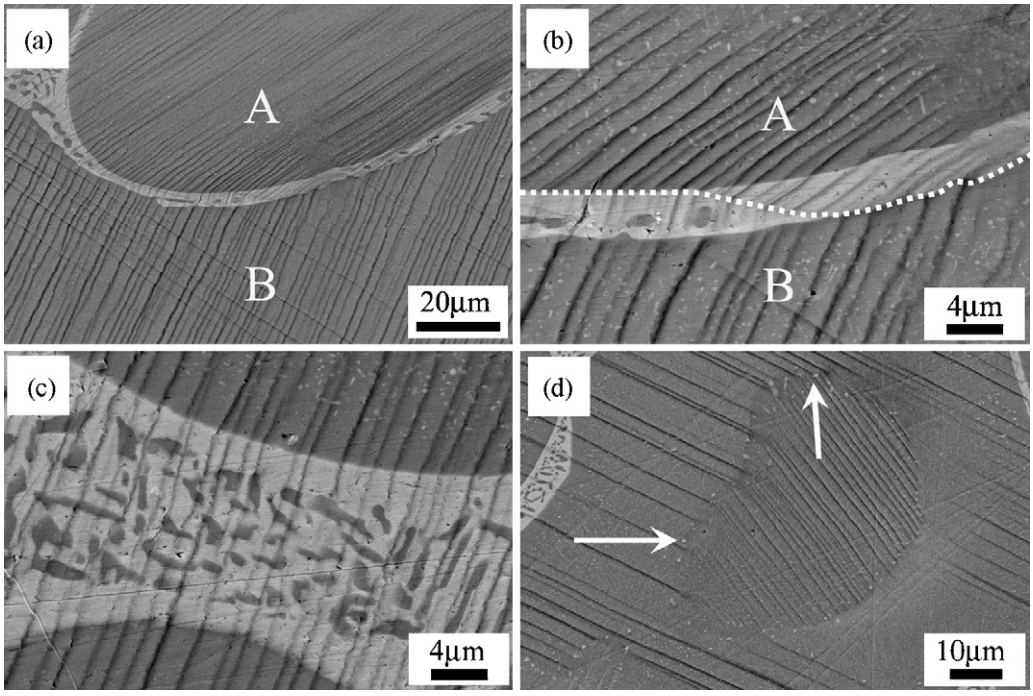

Fig. 6. (a–d) SEM images showing the surface deformation morphologies in region U of the Cu–16 wt.%Ag alloy.

with grains A and B, respectively. Based on the EBSD orientation maps, it is proposed that the eutectic above the broken line may nucleate on grain A, while the eutectic below the broken line may nucleate on grain B. This seems reasonable because near the grain boundary, both grains A and B can act as nucleation sites. Different from the deformation behavior near the grain boundary, the eutectic inside the grain shows the same slip direction as the dendrites (see Fig. 6c), and the slip bands can keep one-to-one relationship. This should be attributed to the same orientation between them, as indicated by the EBSD results in the previous section. The similar lattice parameter and the coplanar slip systems of Cu and Ag are also very important for the continuity of the slip bands. Interestingly, a small region with different slip directions was observed embedding in the Cu matrix (see Fig. 6d). Besides, some coarse precipitates can also be seen at the grain boundary, as indicated by arrows. This is because no eutectic colony distributed between the dendritic arms and two dendrites with different orientations conjoin with each other directly. These special orientations should be corresponding to the EBSD orientation map as shown in Fig. 3b (see the inset rectangle).

From the observations on the slip deformation in detail, it is apparent that the slip deformation within the matrix and near the interfaces has quite good compatibility in the Cu–Ag alloy with coarse-grained microstructure, which makes it display significantly high tensile plasticity. Furthermore, based on the basic understanding of the slip deformation around the interphase interfaces, such two-phase Cu–Ag alloys can be considered to be fabricated into high-performance structural materials with high strength and good ductility in the future.

4. Conclusions

Based on the investigation on the microstructures and tensile deformation behaviors of the two Cu–Ag binary alloys, the following conclusions can be drawn:

(1) EBSD results show that most of the eutectic products have the same orientation as the proeutectic dendrites. Therefore, it is likely that the eutectic component nucleates on the proeutectic dendrites in such areas. In other areas, eutectic component has different orientations from the proeutectic dendrite.
(2) Although the dendrites are abundant in precipitates, slip bands are still observed in dendrites in the deformed samples. This can be attributed to the cube-on-cube orientation relationship and the coplanar slip systems between the precipitates and the dendrites. Slip bands can penetrate through the interphase interfaces between the eutectic region and the dendrites, which can also be attributed to the coplanar slip systems between them.

Acknowledgements

The authors would like to thank W. Gao, Q.Q. Duan, H.J. Yang, P. Zhang, H.F. Zou and P. Li for the assistance in the sample preparation, mechanical tests and SEM observations. This work was financially supported by the National Outstanding Young Scientist Foundation under Grant No. 50625103 and the National Natural Science Foundation (NSFC) of China under Grant No. 50890173.

References

[1] W.D. Callister, Materials Science and Engineering, 2nd ed., John Wiley& Sons, New York, 1985 (an introduction).
[2] D. Dew-Hughes, Mater. Sci. Eng. A 168 (1993) 35.
[3] J.T. Wood, J.D. Embury, M. Ashby, Acta Mater. 45 (1997) 1099.
[4] H.P. Frings, L. Van Bockstal, Physica B 211 (1995) 73.
[5] K. Inoue, T. Asano, T. Kiyoshi, Y. Sakai, T. Takeuchi, K. Itoh, H. Maeda, Physica B 177 (1992) 7.
[6] A. Benghalem, D.G. Morris, Acta Mater. 45 (1997) 397.
[7] Y. Sakai, H.-J. Schneider-Muntau, Acta Mater. 45 (1997) 1017.
[8] Y. Sakai, K. Inoue, T. Asano, H. Wada, H. Maeda, Appl. Phys. Lett. 59 (1991) 2965.
[9] L. Zhang, L. Meng, Scripta Mater. 52 (2005) 1187.
[10] A. Gaganov, J. Freudenberger, W. Grv̈nberger, L. Schultz, Z. Metallkd. 95 (2004) 425.
[11] S. Nagasaki, M. Hirabayashi, Binary Alloy Phase-diagrams, AGNE Gijutsu Center Co. Ltd., Tokyo, Japan, 2002.
[12] J.B. Liu, L. Meng, Y.W. Zeng, Mater. Sci. Eng. A 435–436 (2006) 237.
[13] K. Han, A.A. Vasquez, Y. Xin, P.N. Kalu, Acta Mater. 51 (2003) 767.
[14] G. Rao, J.M. Howe, P. Wynblatt, Scripta Metall. Mater. 30 (1994) 731.
[15] J.B. Liu, Y.W. Zeng, L. Meng, J. Alloys Compds. 464 (2008) 168.
[16] S.I. Hong, M.A. Hill, Acta Mater. 46 (1998) 4111.
[17] K.H. Lee, S.I. Hong, J. Mater. Res. 18 (2003) 2194.
[18] K. Han, A.C. Lawson, J.T. Wood, J.D. Embury, R.B. Von Dreele, J.W. Richardson Jr., Philos. Mag. 84 (2004) 2579.
[19] R.G. Hoagland, T.E. Mitchell, J.P. Hirth, H. Kung, Philos. Mag. A 82 (2002) 643.
[20] D. Raabe, U. Hangen, Compos. Sci. Technol. 55 (1995) 57.
[21] D. Raabe, U. Hangen, Comput. Mater. Sci. 5 (1996) 195.
[22] Y. Leprince-Wang, K. Han, Y. Huang, K. Yu-Zhang, Mater. Sci. Eng. A 351 (2003) 214.
[23] Z.G. Wang, Z.F. Zhang, X.W. Li, W.P. Jia, S.X. Li, Mater. Sci. Eng. A 319–321 (2001) 63.
[24] K. Nogita, A.K. Dahle, Mater. Charact. 46 (2001) 305.
[25] W. Grv̈nberger, M. Heilmaier, L. Schultz, Z. Metallkd. 93 (2002) 58.
[26] A.K. Dahle, J. Hjelen, L. Arnberg, in: J. Beech, H. Jones (Eds.), Proceedings of the Fourth Decennial International Conference on Solidification Processing (SP97), Sheffield, United Kingdom, 1997.
[27] L.M. Hogan, H. Song, Acta Metall. 35 (1987) 677.
[28] J.P. Schaffer, A. Saxena, S.D. Antolovich, T.H. Sanders, S.B. Warner Jr., The Science and Design of Engineering Materials, 2nd ed., McGraw-Hill Companies, 1999.
[29] R. Elliott, Eutectic Solidification Processing, Butterworths & Co (Publishers) Ltd., 1983.